**Joint Polar Satellite System (JPSS) Ground Project
Code 474
474-00051**

Joint Polar Satellite System (JPSS) VIIRS Land Surface Temperature Algorithm Theoretical Basis Document (ATBD)

For Public Release

**Goddard Space Flight Center
Greenbelt, Maryland**

National Aeronautics and
Space Administration

Joint Polar Satellite System (JPSS)
VIIRS Land Surface Temperature
Algorithm Theoretical Basis Document (ATBD)

JPSS Electronic Signature Page

Prepared By:

Neal Baker
JPSS Data Products and Algorithms, Senior Engineering Advisor
(Electronic Approvals available online at (https://jpssmis.gsfc.nasa.gov/mainmenu_dsp.cfm)

Approved By:

Heather Kilcoyne
DPA Manager
(Electronic Approvals available online at (https://jpssmis.gsfc.nasa.gov/mainmenu_dsp.cfm)

Goddard Space Flight Center
Greenbelt, Maryland

i

Preface

This document is under JPSS Ground AERB configuration control. Once this document is approved, JPSS approved changes are handled in accordance with Class I and Class II change control requirements as described in the JPSS Configuration Management Procedures, and changes to this document shall be made by complete revision.

Any questions should be addressed to:

JPSS Ground Project Configuration Management Office
NASA/GSFC
Code 474
Greenbelt, MD 20771

Change History Log

Revision	Effective Date	Description of Changes (Reference the CCR & CCB/ERB Approve Date)
Original	04/22/2011	**474-CCR-11-0066:** This version baselines D43756, VIIRS Land Surface Temperature Algorithm Theoretical Basis Document ATDB (ref Y2399), Rev C, dated 12/22/2010, as a JPSS document, version Rev –. This is the version that was approved for NPP launch. Per NPOESS CDFCB - External, Volume V – Metadata, doc number D34862-05, this has been approved for Public Release into CLASS. This CCR was approved by the JPSS Algorithm ERB on April 22, 2011.
A	06/26/2013	**474-CCR-13-1090:** This CCR was approved by the JPSS Algorithm ERB on June 26, 2013. Abstract, Section 2.1 and 3.3.2 were affected.

Northrop Grumman Corporation
Aerospace Systems
One Space Park
Redondo Beach, CA 90278

Engineering & Manufacturing Development (EMD) Phase
Acquisition & Operations Contract

CAGE NO. 11982

VIIRS Land Surface Temperature
Algorithm Theoretical Basis Document ATBD (ref Y2399)

Document Number: D43756

Document Date: 12/22/2010

Revision: C

PREPARED BY: _____
Justin Ip, Models & Simulations

ELECTRONIC APPROVAL SIGNATURES:

_____   _____

 Roy K Tsugawa, , A&DP IPT Lead

Prepared by
Northrop Grumman Aerospace Systems
One Space Park
Redondo Beach, CA 90278

Prepared for
Department of the Air Force
NPOESS Integrated Program Office
C/O SMC/CIK
2420 Vela Way, Suite 1467-A8
Los Angeles AFB, CA 90245-4659

Under
Contract No. F04701-02-C-0502

iv

COMMERCE DESTINATION CONTROL STATEMENT

The export of these commodities, technology or software are subject to U.S. Export Laws and Regulations in accordance with the Export Administration Regulations. Diversion contrary to U.S. law is prohibited.

Northrop Grumman Aerospace System Corp. One Space Park Redondo Beach, CA 90278	**NORTHROP GRUMMAN** **Raytheon**

Revision/Change Record			**Document Number** D43756	
Revision	**Document Date**	**Revision/Change Description**		**Pages Affected**
---	1/24/2007	Initial PCIM Release to bring document into Matrix Accountability. Reference original document number: Y2399 delivered in 2004		All
A	2/18/2009	Updated according to CSR RFA SY_146 with NGST SPCR ALG00001364 under ECR A201		Most pages
B	12/16/2009	Updates corresponding to ECR A-264 for implementation of an algorithm switch to allow running the LST algorithm using the split window algorithm.		Cover page, pages vi, viii, 1, 2, 3, 6, 7, 33

C	12/22/2010	Updated default (baseline) algorithm mode setting as the two band split window algorithm
		  - updated Abstract section stating that the 2-band algorithm is the default
		  - updated section 1.4 Revisions with statement about Rev C modifications
		  - updates for stating that the 2 band split window algorithm is the default
				p. x
				p. 1-2
				p. 3, 5, 6, 10, 14, 24-26, 28, 30,31,33, 34

LAND SURFACE TEMPERATURE

VISIBLE/INFRARED IMAGER/RADIOMETER SUITE
ALGORITHM THEORETICAL BASIS DOCUMENT

Version 5, Revision 3: November 2004

Richard J. Sikorski
Peter S. Kealy

William Emery, Science Team Member
University of Colorado

RAYTHEON SYSTEMS COMPANY
Information Technology and Scientific Services
4400 Forbes Boulevard
Lanham, MD 20706

SBRS Document #: Y2399

Revision/Change Record			For Document No.	Y2399
Revision	**Document Date**	**Revision/Change Description**		**Pages Affected**
---	11/30/2004	SPCR ALG00000661		p. 1, 29
---	06/09/2004	SPCR ALG00000444		p. ix, 1, 4-8, 10, 17, 28-30
V5r3	4/4/02	Raytheon revision		All

TABLE OF CONTENTS

LIST OF FIGURES

LIST OF TABLES

GLOSSARY OF ACRONYMS

ATBD	Algorithm Theoretical Basis Document
ATSR	Along Track Scanning Radiometer
AVHRR	Advanced Very High Resolution Radiometer
BBR	Band to Band Registration
ECMWF	European Center for Medium-Range Weather Forecast
FIFE	First International Field Experiment
EDR	Environmental Data Record
IGBP	International Geosphere Biosphere Program
IPO	Integrated Program Office
IR	Infrared
ISLSCP	International Satellite Land Surface Climatology Project
LST	Land Surface Temperature
LUT	Look Up Table
LWIR	Longwave Infrared
MODIS	Moderate Resolution Imaging Spectroradiometer
MODTRAN	Moderate Resolution Atmospheric Radiance and Transmittance Model
MOSART	Moderate Spectral Atmosphere Radiance and Transmittance
MTF	Modulation Transfer Function
MWIR	Midwave Infrared
NCEP	National Centers for Environment Prediction
NFR	Near Field Response
NPOESS	National Polar-orbiting Operational Environmental Satellite System
P^3I	Pre-Planned Product Improvement
PW	Precipitable Water
SBRS	Santa Barbara Remote Sensing
SDR	Sensor Data Record
SSM/I	Special Sensor Microwave Imager
SST	Sea Surface Temperature

TIR	Thermal Infrared
TOA	Top of Atmosphere
VIIRS	Visible/Infrared Imager/Radiometer Suite

ABSTRACT

This is the Algorithm Theoretical Basis Document (ATBD) for the National Polar-orbiting Operational Environmental Satellite System (NPOESS) Visible/Infrared Imager/Radiometer Suite (VIIRS) Land Surface Temperature (LST) algorithm for retrieval of the LST Environmental Data Record (EDR).

The VIIRS LST algorithms are based on physical regression methods to retrieve skin LST. They use brightness temperatures sensed by VIIRS Infrared (IR) channels. The VIIRS baseline LST algorithm is a two band thermal split window algorithm that is based on one equation for each land cover type. A dual split window algorithm that is based on four thermal brightness temperature bands is also available and may be optionally selected to supersede the baseline two band split window algorithm under the most optimum retrieval conditions (i.e., not affected by sun-glint). These algorithms do not require emissivity information.

The atmospheric correction, the complexity of land surface types, and the sensor performance limit the accuracy of satellite LST measurements. The VIIRS LST algorithm requires 2.5 K measurement accuracy and 1.4 K measurement precision. The VIIRS two-band split window and four-band dual split window algorithms (Land cover approach) will likely meet the accuracy requirement for all the land cover types, but may probably miss the 1.4 K precision requirement for some land types.

The validation of LST is limited by the availability of *in situ* observations. The VIIRS LST is defined as the skin temperatures of the uppermost layer of the land surface, while *in situ* observations are usually shelter temperatures. Reliable observed or analyzed skin temperatures will be a critical factor in validating the VIIRS LST retrieval.

1.0   INTRODUCTION

1.1 PURPOSE

This document describes the theoretical basis and development process of the LST algorithms, for retrieval of the LST Environmental Data Record (EDR).

1.2 SCOPE

LST is an input variable for other VIIRS products, such as soil moisture. The LST algorithms described in this document will be used to routinely retrieve LST from VIIRS measurements.

The next section of this document provides an overview of the LST retrieval algorithm. A description of the algorithms and their development is presented in Section 3. Section 3 also addresses error budgets, algorithm sensitivity, and validation. Section 4 identifies the constraints, assumptions, and limitations of the algorithm, and Section 5 presents references cited in this document.

1.3 VIIRS DOCUMENTS

This document contains references to other documents for VIIRS with document numbers:

[SY15-0007] VIIRS System Specification

[PS154640-101] VIIRS Sensor Specification

[D43311] VIIRS Sea Surface Temperature ATBD

[D43759] VIIRS Surface Type ATBD

[Y2469] VIIRS Context Level Software Architecture document

[Y2471] VIIRS Aerosol Module Level Software Architecture

[Y2479]   VIIRS Build SDR Module Level Software Architecture

[Y2502] Land Surface Temperature Unit Level Detailed Design

[Y2473] VIIRS Surface Temperature Module Level Software Architecture document

[D43777] VIIRS Radiometric Calibration ATBD

[Y3277] VIIRS Aerosol Module Level Interface Control Document

[Y10880]   VIIRS Surface Temperature IP Unit Level Detailed Design Document

[D45702] NPP Operational Algorithm Proxy and Synthetic Test Data Description document

[D37005] VIIRS EDR Production Report

[D36385] VIIRS EDR Interdependency Report

1

[D38714] VIIRS Operational Algorithm Description Document for the VIIRS Land Surface Temperature EDR

1.4 REVISIONS

This is revision C of this document document since its initial release by NGST after its adaption from the Version 5 Revision 5 of the Raytheon document, dated November 2004. This revision provides updates for specification of the two band split window LST algorithm as the operational default algorithm mode. Revision B of this document provided updates for an algorithm switch for optional selection of the two band split window algorithm. This current version is maintained by NGST and has been updated by Algorithm, Model and Simulation since Version 2, Revision 2. Substantial contributions to prior versions of this document were made by Donglian Sun, Yimin Ji, Philip E. Ardanuy, and Wenli Yang.

2.0   EXPERIMENT OVERVIEW

2.1 OBJECTIVES OF LAND SURFACE TEMPERATURE RETRIEVALS

Land surface temperatures play an important role in land-surface processes on a regional as well as on a global scale. They are of fundamental importance to the net radiation budget at the Earth's surface and to monitoring the state of crops. LST is a good indicator of both the greenhouse effect and the energy flux between the atmosphere and the ground (Mannstein, 1987; Sellers *et al*., 1988). Satellite-derived LST assimilates to climate, mesoscale and land surface models to estimate the sensible heat flux and latent heat flux from the Earth's surface. Satellite-based LST measurement has not been used operationally in regional weather forecasting and climate prediction due to large uncertainties. However they have the potential to provide LST information over vast remote regions such as deserts.

The accuracy of satellite LST measurement is primarily limited by the complexity of land surface types, the atmospheric correction, and sensor performance. The published satellite multichannel LST algorithm permits global LST retrievals within 3 to 4 K measurement accuracy (Becker and Li, 1990; Dozier and Wan, 1994; Li and Becker, 1993).

The overall scientific objective of the VIIRS LST retrieval is to provide improved measurements of global and regional LST fields.

2.2 INSTRUMENT CHARACTERISTICS

The VIIRS sensor has been designed based on the NPOESS sensor requirements derived from EDR system specifications. VIIRS bands in the Longwave Infrared (LWIR) region have been placed to optimize their use for Sea Surface Temperature (SST) determination. Bands in the LWIR are usually located near the maximum Earth radiance. The influence of ozone and other atmospheric absorbers should be avoided. Figure 1 shows the Moderate Resolution Atmospheric Radiance and Transmittance Model (MODTRAN) simulated radiances at satellite altitude for thermal infrared spectra. There are a total of five standard atmospheres shown. There are two wavelength regions suitable for LWIR band selection: 8–9 μm and 10–13 μm. VIIRS LWIR bands are located in the two spectral regions. Figure 2 shows the MODTRAN simulated atmospheric transmittance for five standard atmospheres. It shows that the 8–9 μm and 10–13 μm regions are transparent to the atmosphere. The details of LST band selection can be found in Caselles *et al*., 1997, however VIIRS bands were optimized for SST.
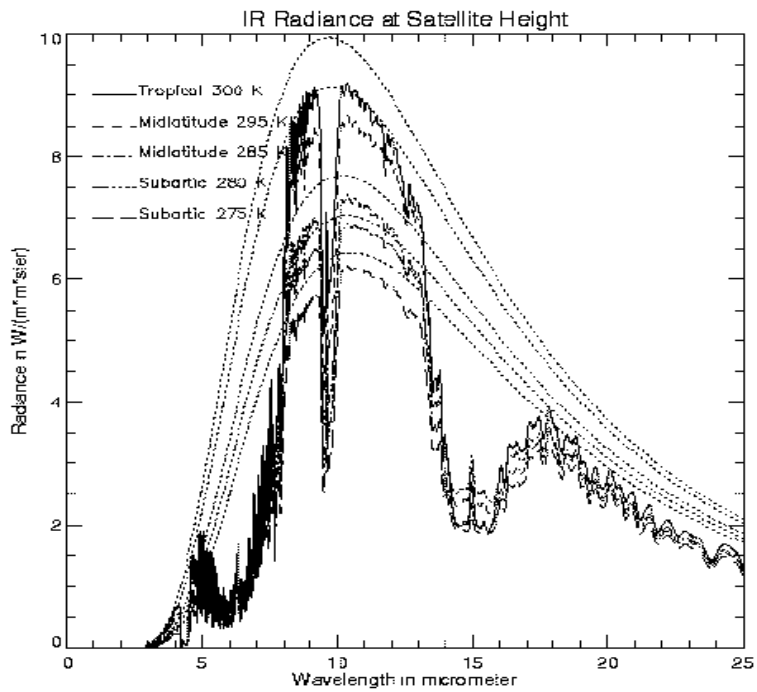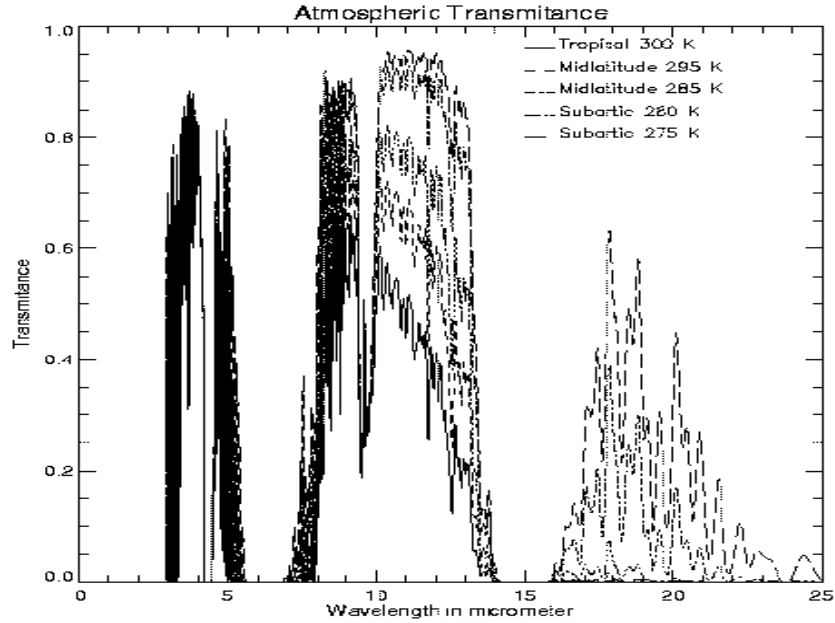
3

Figure 1. IR radiance at the satellite for five atmospheres simulated by MODTRAN. The dashed lines are calculated from the Planck function.

4

**Figure 2. Atmospheric transmittances for five atmospheres.
The dashed lines are calculated from the Planck function.**

2.3 LAND SURFACE TEMPERATURE RETRIEVAL STRATEGIES

If we were to solve the LST problem physically, we would have to know the atmospheric profile for each pixel (unlikely to be available operationally in the near future), and also the surface emissivity for each band. Because the surface emissivity for each band is different, the number of unknowns is always larger than the number of equations. A number of ways have been suggested to physically retrieve the surface temperature and emissivity. These methods include the two-temperature method (Watson, 1992), the temperature emissivity separation method (Kealy and Hook, 1993), and the day/night method (Wan and Dozier, 1996). However, these methods demand many more LWIR bands than in the VIIRS baseline design

VIIRS testbed results have shown that Land Cover regression methods, with a separate set of coefficients for each land cover type, are able to meet requirements by compensating for variations in emissivity among surface types.

Land Cover Approach Regression methods

1A. Two band Algorithm (Baseline Algorithm):

For each of the 17 IGBP surface types, establish one equation by using 11 and 12 μm split window.

$$LST_i = a_0(i) \quad + a_1(i)\,T_{11} + a_2(i)\,(T_{11} - T_{12}) + a_3(i)\,(\sec\theta - 1) + a_4(i)\,(T_{11} - T_{12})^2 \qquad i = 1,...,17$$

$$(3)$$

The two band split window algorithm is less sensitive to band to band (BBR) mis-registration and near field (NFR) scattering sensor effects then the optional four band algorithm.

1B. Four band Algorithm (Optional Algorithm):

VIIRS dual split window day/night LST algorithm establishes one equation for each surface type by using 4 VIIRS bands (10.8, 12, 3.75, and 4.005 μm), with added solar zenith angle correction during the daytime:

Daytime:

$$LST_i = a_0(i) + a_1(i)T_{11} + a_2(T_{11} - T_{12}) + a_3(i)(\sec\theta - 1) + a_4(i)T_{3.75} + a_5(i)T_{4.0} + a_6(i)T_{3.75}\cos\varphi$$
$$+ a_7(i)T_{4.0}\cos\varphi + a_8(i)(T_{11} - T_{12})^2 \qquad i = 1,...,17 \tag{1}$$

Nighttime:

$$LST_i = b_0(i) + b_1(i)T_{11} + b_2(T_{11} - T_{12}) + b_3(i)(\sec\theta - 1) + b_4(i)T_{3.75} + b_5(i)T_{4.0} + b_6(i)T_{3.75}{}^2$$
$$+ b_7(i)T_{4.0}{}^2 + b_8(i)(T_{11} - T_{12})^2 \qquad i = 1,...,17$$

(2)

where i is the index of the 17 International Geosphere Biosphere Program (IGBP) surface types (Table 2). For more details see the VIIRS Surface Type ATBD, D43759. LST_i are the land surface temperatures for the ith IGBP surface type. T_{11}, T_{12}, $T_{3.75}$, and $T_{4.0}$ are the brightness temperatures of the VIIRS 10.8, 12, 3.75, and 4.0 µm bands respectively. θ and φ are the sensor and solar zenith angles respectively. $a_j(i)$ and $b_j(i)$ are the regression coefficients for the jth IBGP surface type for daytime and nighttime LST retrievals respectively.

The four band split window algorithm may be optionally selected to supersede the baseline split window algorithm if its performance is determined to be better than the baseline algorithm.

3.0   ALGORITHM DESCRIPTION

The VIIRS cloud cover, snow/ice, and land/ocean masks are used to eliminate cloud-contaminated, ice-covered, and ocean pixels. Land cover type is retrieved from visible and near-IR bands by the VIIRS Land software module. The LST is retrieved using a regression equation, with separate coefficients for each land cover type. For the VIIRS baseline split window algorithm, only knowledge of the land type is needed and no emissivity information is required.

3.1 PROCESSING OUTLINE

The coefficients for the regression equations will be obtained using MODTRAN and a global database through our simulation processes. Figure 3 depicts the processing concept for LST retrievals. In the VIIRS baseline dual split window algorithm, one equation is developed for each of the 17 IGBP land cover types for operational use (Figure 3; Table 2).
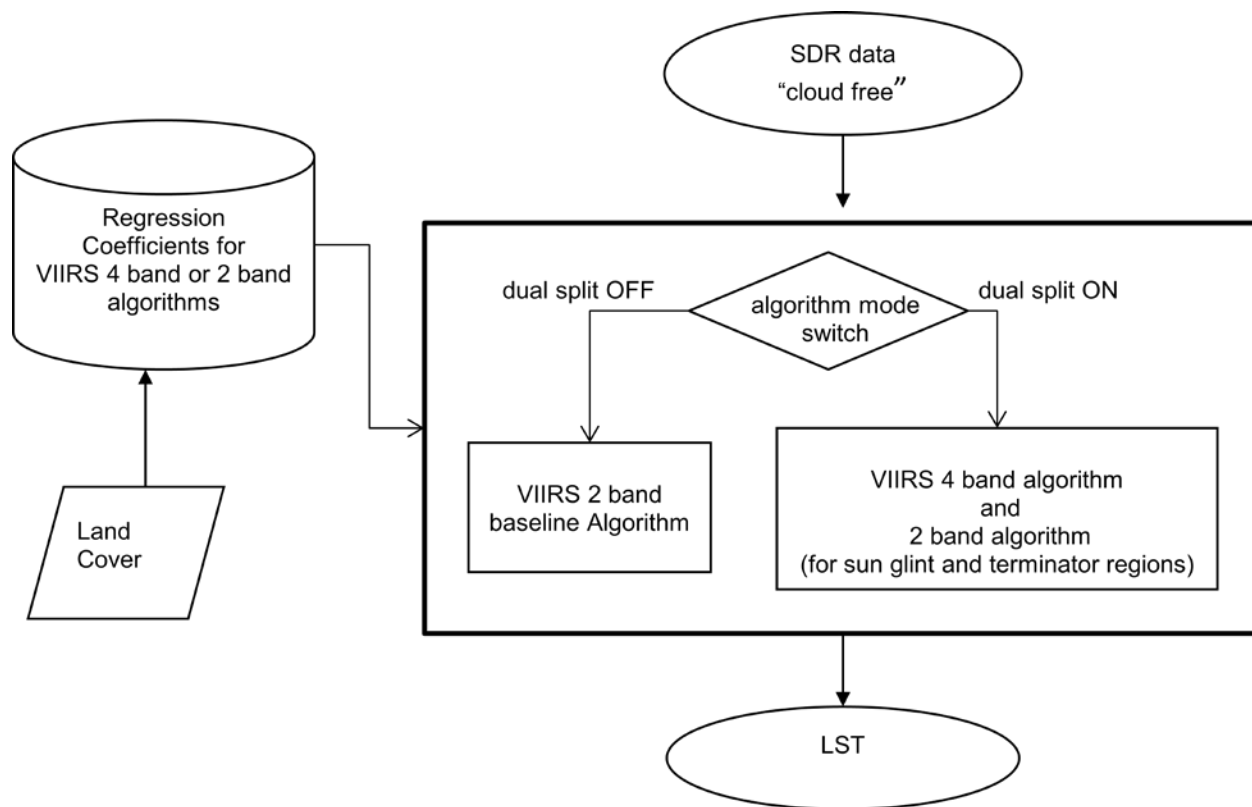
Figure 3. LST flowchart: Land cover approach - One equation for each land surface type.

3.2 ALGORITHM INPUT

3.2.1 VIIRS Data

VIIRS inputs required for the LST algorithm are Land Cover classification, brightness temperatures from the IR bands, cloud mask, ice/snow mask, and land/ocean mask.

3.2.2 Non-VIIRS Data

The operational VIIRS LST algorithms do not require non-VIIRS data.

3.2.2 Regression Coefficients

The VIIRS LST algorithms also require regression coefficients for each IGBP land cover type for day and night for baseline and fallback algorithms.

3.3 THEORETICAL DESCRIPTION OF LAND SURFACE TEMPERATURE RETRIEVAL

3.3.1 Physics of the Problem

In clear sky conditions, the outgoing infrared spectral radiance at the top of atmosphere can be represented by:

$$L(\lambda,\mu) = \tau(\lambda,\mu)\varepsilon(\lambda,\mu)B(\lambda,T_s) + L_a(\lambda,\mu) + L_s(\lambda,\mu,\mu_0,\varphi_0)$$
$$+ L_d(\lambda,\mu,\mu_0,\varphi_0) + L_r(\lambda,\mu,\mu_0,\varphi_0) \tag{4}$$

where τ is the transmissivity, ε the surface spectral emissivity, B the Plank function, L_a the thermal path radiance, L_s the path radiance resulting from scattering of solar radiation. L_d is the solar radiance and L_r the solar diffuse radiation and atmospheric thermal radiation reflected by the surface. λ is the wavelength. $\mu = \cos(\theta)$, $\mu_o = \cos(\psi)$, where θ is the satellite zenith angle, ψ the solar zenith angle. φ_o is the azimuth angle.

The wavelength is the wavelength center of a narrow interval because there is no way to measure the exact monochromatic signal as a continuous function of wavelength by satellite sensors. Equation 4 can be used in the 3–14 μm range. It requires complete calculations of the atmospheric radiative transfer to determine the values of all terms on the right side. This equation has been used in many atmospheric radiation models including LOWTRAN (Kneizys *et al*., 1988), MODTRAN (Berk *et al*., 1987), and Moderate Spectral Atmospheric Radiance and Transmittance (MOSART) (Cornette *et al*., 1994).

8

For LWIR bands, L_d, L_s, and L_r are negligible. Therefore, only the first two terms on the right side of the above equation are important. The first term represents the surface contribution term, and it is the gray-body radiance emitted by the earth's surface. The second term is the atmospheric contribution term, and is the vertically integrated effect of emission from every atmospheric layer modulated by the transmittance of the air above that emitting layer.

$$L(\lambda,\mu) = \varepsilon_0(\lambda,\mu)B(\lambda,T_s)\tau_0(\lambda,\mu) + \int_{\tau_0}^{1} B(\lambda,T_p)d\tau(\lambda,\mu,\rho) \qquad (5)$$

where τ_0 is the transmittance at the Earth's surface.

In order to infer the surface information, we should choose window channels with small atmospheric contributions. As shown in Figure 1, the wavelength between 3.5–4.2 μm, 8–9 μm, and 10–13 μm are some typical atmospheric windows, with less atmospheric absorption. For a perfect window, the total atmospheric transmittance $\tau_0(\lambda\ \mu)$ should be 1.0, and the transmittance weighting function should be 0. But as we see from Figure 2, the transmittances at these windows are not 1.0. This is mainly the result of the water vapor absorption.

In order to see the water vapor's contribution at the atmospheric window channel, we did some simulations to the 2415 profiles offered by the IPO over land surfaces under clear sky conditions by using MODTRAN 3.7. The following five window bands are simulated: 3.75 μm, 10.8 μm (AVHRR channel 4), 12 μm (AVHRR channel 5), and two new VIIRS bands, including 4.005 μm and 8.55 μm.

As we can see from the transmittance vs. surface skin temperature distribution, shown as Figure 4a, at warmer temperatures (285–310 K), for 10.8 and 12 μm channels and the 8.55 μm channel, the transmittances decrease significantly. Most values are below 0.8. This is why most existing split window algorithms using the 11 and 12 μm channels get larger errors in the temperature range 285–310 K. The transmittance for the Midwave Infrared (MWIR) channel 3.75 μm and 4.005 μm is more stable, with less change to the surface skin temperature; most values are above 0.8. From this aspect, MWIR 3.75 μm and 4.005 μm channels are better window channels than the LWIR 11, 12, and 8.55 μm channels. The most stable channel is at 4.005 μm. From the transmittance vs. PW (Figure 4b), we can also see that the transmittance at the 4.005 μm channel is the most stable. It changes very little with the column water vapor amount. While the transmittance at 3.75 μm channel has a linear relationship with the precipitable water, the transmittances at 11, 12, and 8.55 μm decrease significantly as the water vapor increases and the relationship is also not linear. The information from MWIR window channel can be used when we retrieve warmer surface temperatures.

From the difference between the surface temperature and brightness temperature vs. precipitable water distribution, as shown in Figure 4c, the temperature deficit (Ts-Tb) at IR window channels 11, 12, and 8.55 μm is very stable, while the surface temperature at MWIR

9

channels 3.75 and 4.005 μm can be much lower than the brightness temperature, sometimes by more than 10 degrees. This is because in the daytime, the MWIR channel contains both reflected solar radiation and radiation emitted by the surface and the atmosphere, this is the so-called solar glint. It is therefore potentially advantagous to retrieve surface temperature based on a combination of LWIR and MWIR window channels.

10
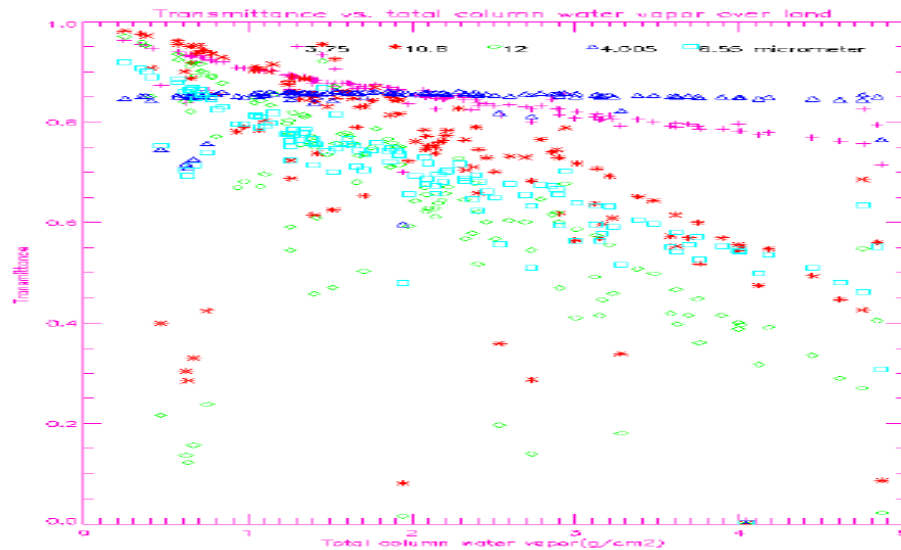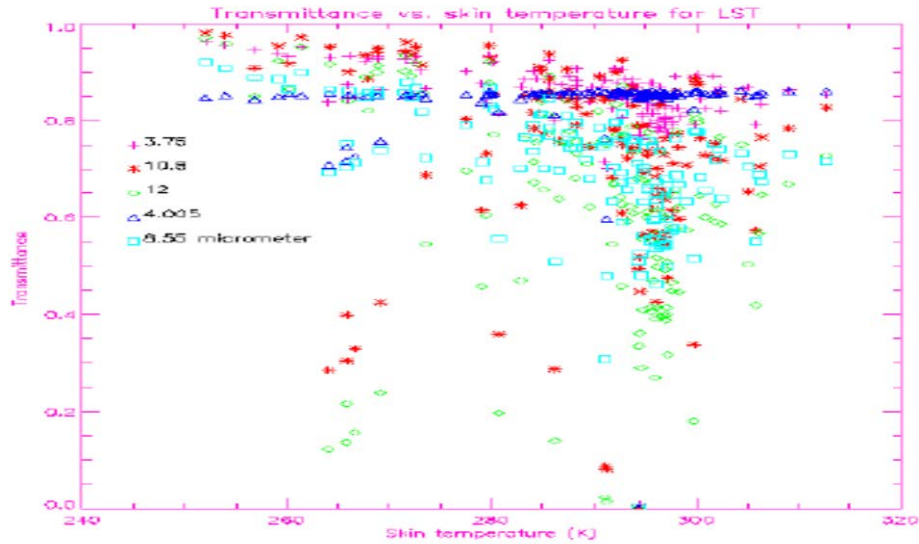
Figure 4a. Upper Panel: Transmittance vs. LST. 4b. Lower Panel: Transmittance vs. PW over land.
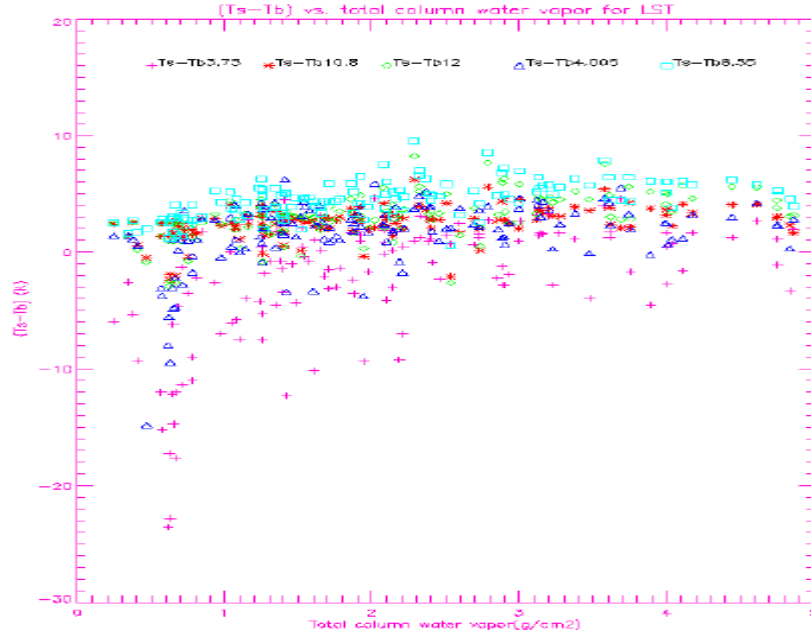
Figure 4c. Temperature deficits (T_s-T_b) vs. PW distribution.

Currently, most existing LST algorithms are variants based on Becker and Li's split window technique (1990).

$$Ts = (A_1 + A_2 \frac{1-\varepsilon}{\varepsilon} + A_3 \frac{\Delta\varepsilon}{\varepsilon^2})\frac{T_{11} + T_{12}}{2} + (B_1 + B_2 \frac{1-\varepsilon}{\varepsilon^2} + B_3 \frac{\Delta\varepsilon}{\varepsilon^2})(T_{11} - T_{12}) + C \tag{6}$$

where $\varepsilon = (\varepsilon_{11} + \varepsilon_{12})/2$ and $\Delta\varepsilon = \varepsilon_{11} - \varepsilon_{12}$. ε_{11} and ε_{12} are the emissivities at 10.8 μm and 12 μm bands respectively; T_{11} and T_{12} are the brightness temperatures at 10.8 μm and 12 μm bands respectively; A_1, A_2, A_3, B_1, B_2, B_3, and C are regression coefficients.

One of the major difficulties in the development of the LST algorithm is the considerable spectral variation in emissivities for different land surface types. Observation of emissivity

11

spectra shows that in general, emissivity spectra with high values exhibit little variation, while those with lower values exhibit a greater variation, such as grass, as shown in Figure 5.
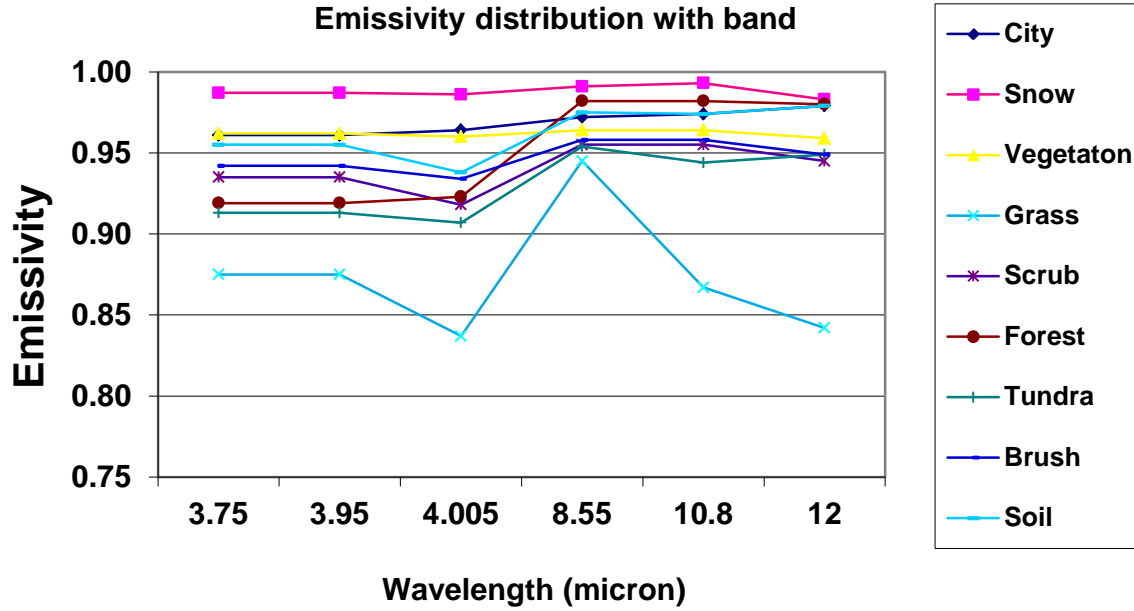
Figure 5. Variation in emissivity for different surface types.

If we ignore the change of emissivity for a certain land surface type, the radiance error introduced by the atmosphere ΔL can be represented by:

$$\Delta L = B(\lambda, T_s) - L(\lambda, \mu) = B(\lambda, T_s) - \tau(\lambda, \mu)B(\lambda, T_s) - L_a(\lambda, \mu)$$
$$= -\int_1^{\tau(\lambda,\mu)} B(\lambda, T_s)d\tau(\lambda, \mu, p) + \int_1^{\tau(\lambda,\mu)} B(\lambda, T_p)d\tau(\lambda, \mu, p) \qquad (7)$$
$$= -\int_1^{\tau(\lambda,\mu)} (B(\lambda, T_s) - B(\lambda, T_p))d\tau(\lambda, \mu, p)$$

From the Planck function we find:

$$\Delta L = \frac{\partial B}{\partial T}\Delta T = \frac{\partial B}{\partial T}(T_s - T_\lambda) \qquad (8)$$

12

For an optically thin gas the following approximations can be made:

$$\dot{}\, d\tau = d\{\exp(-k_\lambda L)\} = -k_\lambda dl \tag{9}$$

where k_λ is the absorption coefficient and l is the optical path-length.

If we assume that the Planck function is adequately represented by a first order Taylor series expansion in each channel window, then:

$$B(\lambda,T_s) - B(\lambda,T_p) = \left.\frac{\partial B(\lambda,T_p)}{\partial T}\right|_{T_s} (T_p - T_s) \tag{10}$$

Substituting Equations 8, 9, 10 into Equation 7, we obtain:

$$T_s - T_\lambda = k_\lambda \int_1^\tau (T_s - T_p) dl \tag{11}$$

Therefore, if we select two spectral regions of the atmosphere, we will have two linear equations with different k_λ to solve simultaneously.

For example if we consider the two channels as $\lambda=1$ and $\lambda=2$, then we get:

$$T_s - T_1 = -(T_2 - T_1)k_1 / (k_2 - k_1) \tag{12}$$

This equation is similar to the SST equation, but can only be used for one land type, assuming the band emissivity does not vary within this land type. Figure 6a shows the relationship between band temperature deficits T_s-T_{11} and T_s-T_{12} for forests. The data are global data with 17,885 skin temperatures and atmospheric profiles. The relationship is rather linear, which confirms that for a particular land type, the linear split window algorithm used in SST retrieval can be adopted for LST. Figure 6b is similar to Figure 6a, but for simulations of 23 land cover types. There is much more variation in this figure; the relationship is not linear. Emissivities, therefore, have to be considered as an important factor for Becker and Li's 1990 LST algorithm.

For land surfaces, the emissivity for each channel changes with surface type. Table 1 shows the band-averaged emissivities for the 23 VIIRS testbed surface types derived from MOSART spectra. The VIIRS testbed surface types contain a majority of the IGBP land surface types. The VIIRS LAND EDR will deliver the 17 IGBP land surface types for operational LST retrieval (Table 2). The difference between the 10.8 µm and 12 µm band emissivities for a particular surface type is small for most of the types, thus a land cover approach making the use of separate sets of coefficients for each land type is feasible.
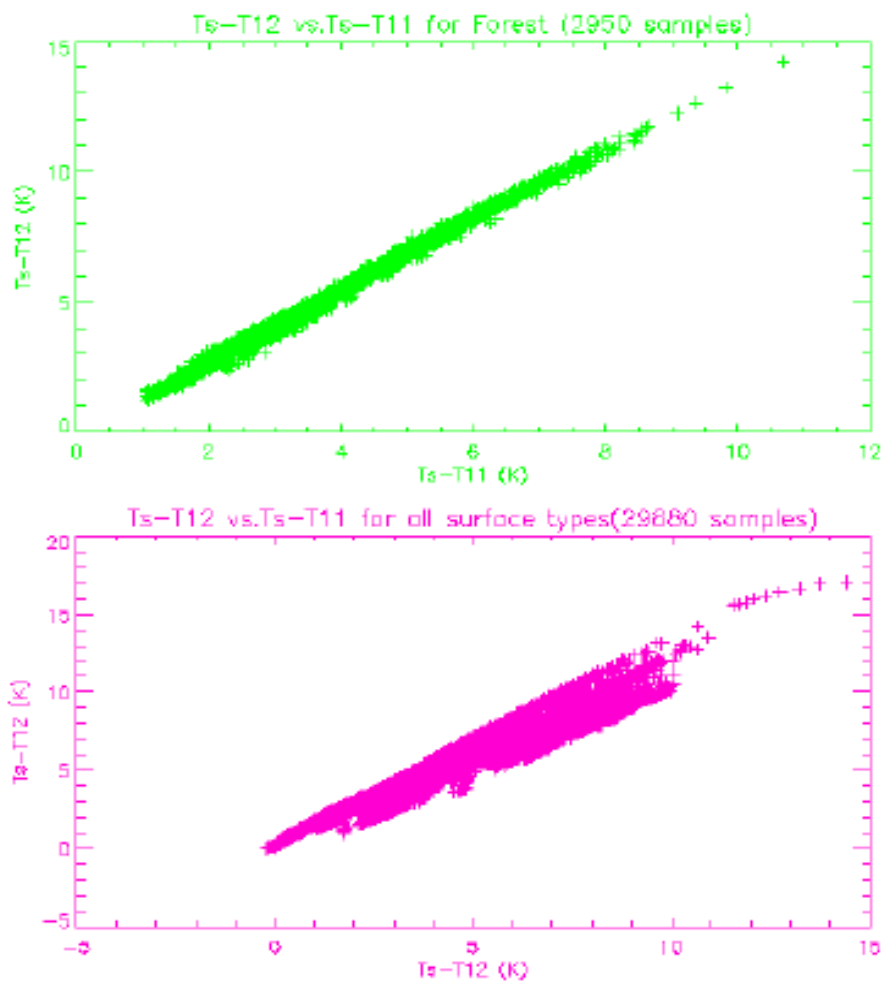
Figure 6. (a) Relationship between temperature deficits of 10.8 μm and 12 μm bands for forest only. (b) Relationship between temperature deficits of 10.8 μm and 12 μm bands for the 23 VIIRS testbed land types.

Table 1. Band-Averaged Emissivities of 23 Surface Types in VIIRS testbed Bands 10, 11, 12, SST1, SST2, SST4.

Surface Type Index	Type of Materials	$\varepsilon_{3.75}$	$\varepsilon_{10.8}$	ε_{12}	$\varepsilon_{3.99}$	$\varepsilon_{4.00}$	$\varepsilon_{8.55}$
1	Water	0.980	0.990	0.990	0.980	0.980	0.985
2	Old snow	0.987	0.993	0.983	0.987	0.986	0.991
3	Sea ice	0.987	0.995	0.983	0.987	0.982	0.992
4	Compacted soil	0.930	0.957	0.967	0.930	0.895	0.965
5	Tilled soil	0.951	0.970	0.977	0.951	0.926	0.975
6	Sand	0.500	0.950	0.980	0.500	0.550	0.900
7	Rock	0.800	0.915	0.960	0.800	0.840	0.895
8	Cropland	0.962	0.964	0.959	0.962	0.960	0.964
9	Meadow grass	0.875	0.867	0.842	0.875	0.837	0.945
10	Scrub	0.935	0.955	0.945	0.935	0.918	0.955
11	Broadleaf forest	0.952	0.962	0.956	0.952	0.957	0.962
12	Pine forest	0.905	0.990	0.990	0.905	0.907	0.990
13	Tundra	0.913	0.944	0.949	0.913	0.907	0.954
14	Grass-soil	0.908	0.921	0.918	0.908	0.872	0.957
15	Broadleaf-pine forest	0.919	0.982	0.980	0.919	0.923	0.982
16	Grass-scrub	0.905	0.911	0.893	0.905	0.877	0.950
17	Soil-grass-scrub	0.915	0.929	0.923	0.915	0.885	0.956
18	City	0.961	0.974	0.979	0.961	0.964	0.972
19	Pine-brush	0.920	0.973	0.967	0.920	0.913	0.973
20	Broadleaf-brush	0.942	0.958	0.949	0.942	0.934	0.958
21	Wet soil	0.955	0.974	0.979	0.955	0.938	0.975
22	Scrub-soil	0.932	0.956	0.959	0.932	0.904	0.961
23	Broadleaf (70%)—Pine (30%)	0.938	0.970	0.966	0.938	0.942	0.970

15

Table 2. IGBP surface type definitions (from Strahler et al., 1996a).

IGBP Surface Type Names	Definition
1) Evergreen Needleleaf Forests	Lands dominated by woody vegetation with a percent cover >60% and height exceeding 2 meters. Almost all trees remain green all year. Canopy is never without green foliage.
2) Evergreen Broadleaf Forests	Lands dominated by woody vegetation with a percent cover >60% and height exceeding 2 meters. Almost all trees and shrubs remain green year round. Canopy is never without green foliage.
3) Deciduous Needleleaf Forests	Lands dominated by woody vegetation with a percent cover >60% and height exceeding 2 meters. Consists of seasonal needleleaf tree communities with an annual cycle of leaf-on and leaf-off periods.
4) Deciduous Broadleaf Forests	Lands dominated by woody vegetation with a percent cover >60% and height exceeding 2 meters. Consists of broadleaf tree communities with an annual cycle of leaf-on and leaf-off periods.
5) Mixed Forests	Lands dominated by trees with a percent cover >60% and height exceeding 2 meters. Consists of tree communities with interspersed mixtures or mosaics of the other four forest types. None of the forest types exceeds 60% of landscape.
6) Closed Shrublands	Lands with woody vegetation less than 2 meters tall and with shrub canopy cover >60%. The shrub foliage can be either evergreen or deciduous.
7) Open Shrublands	Lands with woody vegetation less than 2 meters tall and with shrub canopy cover between 10-60%. The shrub foliage can be either evergreen or deciduous.
8) Woody Savannas	Lands with herbaceous and other understory systems, and with forest canopy cover between 30-60%. The forest cover height exceeds 2 meters.
9) Savannas	Lands with herbaceous and other understory systems, and with forest canopy cover between 10-30%. The forest cover height exceeds 2 meters..
10) Grasslands	Lands with herbaceous types of cover. Tree and shrub cover is less than 10%.
11) Permanent Wetlands	Lands with a permanent mixture of water and herbaceous or woody vegetation. The vegetation can be present in either salt, brackish, or fresh water.
12) Croplands	Lands covered with temporary crops followed by harvest and a bare soil period (*e.g.*, single and multiple cropping systems). Note that perennial woody crops will be classified as the appropriate forest or shrub land cover type.
13) Urban and Built-Up Lands	Lands covered by buildings and other man-made structures.
14) Cropland/Natural Vegetation Mosaics	Lands with a mosaic of croplands, forests, shrubland, and grasslands in which no one component comprises more than 60% of the landscape.

16

15) Snow and Ice	Lands under snow/ice cover throughout the year.
16) Barren	Lands with exposed soil, sand, rocks, or snow and never has more than 10% vegetated cover during any time of the year.
17) Water Bodies	Oceans, seas, lakes, reservoirs, and rivers. Can be either fresh or salt-water bodies.

17

Figure 7 shows the emissivity change as a function of surface types for four VIIRS MWIR and LWIR bands. LWIR band emissivities are relatively stable for all land types. The changes of MWIR emissivity are larger at land type 6 (sand) and type 7 (rock).

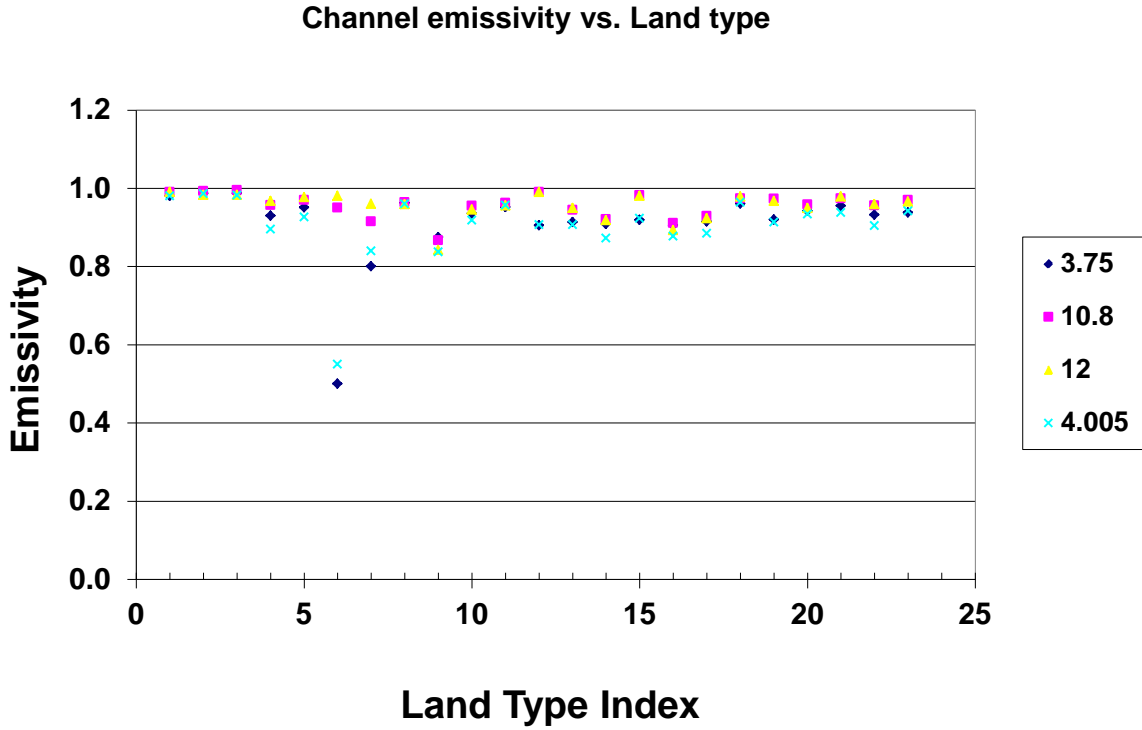**Channel emissivity vs. Land type**

Figure 7. Channel emissivities for 23 land types.

In general, Equation 11 can be written as:

$$T_s = CT_b$$

The coefficient vector C, relating observed brightness temperatures to LST, is determined using a regression method by solving:

$$C = YX^T(XX^T)^{-1} \tag{13}$$

The **Y** matrix contains a large number of training LSTs and the **X** matrix contains brightness temperatures from VIIRS LWIR and MWIR channels. In general, the **X** matrix may include non-linear terms.

Currently, the LST uncertainty from the regression algorithm is about 1 ~ 3 K.

3.3.2 Mathematical Description of the Algorithm

Based on the previous section's discussion of the physics of the problem, the mathematical descriptions of the algorithm can be simply stated.

*Baseline **Split Window** Algorithm:*

The baseline LST algorithm two band split window (11 and 12 μm) algorithm. Regression coefficients are required for each of the 17 IGBP surface types.

$$LST_i = a_0(i) + a_1(i)\,T_{11} + a_2(i)\,(T_{11} - T_{12}) + a_3(i)\,(\sec\theta - 1) + a_4(i)\,(T_{11} - T_{12})^2 \quad i = 1,...,17 \quad (14)$$

Optional Dual Split Window Algorithm:

VIIRS dual split window day/night LST algorithm establishes one equation to each surface type by using 4 VIIRS bands (10.8, 12, 3.75, and 4.005 μm), and it added a solar zenith angle correction during the daytime:

Daytime:

$$LST_i = a_0(i) + a_1(i)T_{11} + a_2(T_{11} - T_{12}) + a_3(i)(\sec\theta - 1) + a_4(i)T_{3.75} + a_5(i)T_{4.0} + a_6(i)T_{3.75}\cos\psi$$
$$+ a_7(i)T_{4.0}\cos\psi + a_8(i)(T_{11} - T_{12})^2 \qquad i = 1,...,17 \tag{15}$$

Nighttime:

$$LST_i = b_0(i) + b_1(i)T_{11} + b_2(T_{11} - T_{12}) + b_3(i)(\sec\theta - 1) + b_4(i)T_{3.75} + b_5(i)T_{4.0} + b_6(i)T_{3.75}{}^2$$
$$+ b_7(i)T_{4.0}{}^2 + b_8(i)(T_{11} - T_{12})^2 \qquad i = 1,...,17 \tag{16}$$

Where *i* is the index of the 17 International Geosphere Biosphere Program (IGBP) surface types (Table 2) produced by the VIIRS Surface Type EDR, θ is the satellite zenith angle and is ψ the solar zenith angle. The two band split window algorithm is used for all sunglint affected pixels.

19

3.3.3 Test Data Set Description

The Test Data Sets we used to develop the VIIRS LST algorithms are described in earlier versions of this document.   Simulations presented here used National Center for Environmental Prediction (NCEP) global snapshot surface temperature data set with matching atmospheric profiles at the resolution 2.5 x 2.5 degrees;

NCEP global snapshot surface temperature data set

The global snapshot surface temperature data set is at 2.5^{o} by 2.5^{o} resolution supplied by the National Centers for Environment Prediction (NCEP), with matching atmospheric profiles.

3.3.4 Variance and Uncertainty Estimates

There are mainly three geophysical factors that contribute to the uncertainty of satellite LST retrieval: land surface classification, emissivity determination errors and atmospheric correction errors. In addition sensor errors need to be accounted for.

Land cover approach

For a specific surface type, the deficits between the surface temperature and the brightness temperature at 11 μm and 12 μm have very good linear relationship, therefore split window algorithms can be adopted to a specific surface type. Land Cover Maps exist and will be improved during the MODIS era, Figure 8. For each surface type, we establish one set of regression coefficients between the surface temperature and 11μm and 12 μm brightness temperature. Figure 9a displays the LST precision for different land surface types. The lines present the results from the VIIRS baseline split window algorithm for various land surface types (Land cover approach). This figure shows that the Land Cover method can improve the retrieval precision for all surface types. Figure 9b shows the summary statistics of retrieval for all the surface types vs. different sensor noise models (the sensor noise increases with noise model). The sensor noise level specification is equivalent to noise model 3.

Figure 10 shows the utility of a solar zenith correction function being added to the equation during daytime retrievals, using the VIIRS optional dual split window algorithm (Land cover approach). The solar zenith correction is particularly useful at higher temperatures. Figure 11 and Figure 12 show the estimated performances of the optional algorithm as a function of viewing angle and temperature for both day and night respectively.
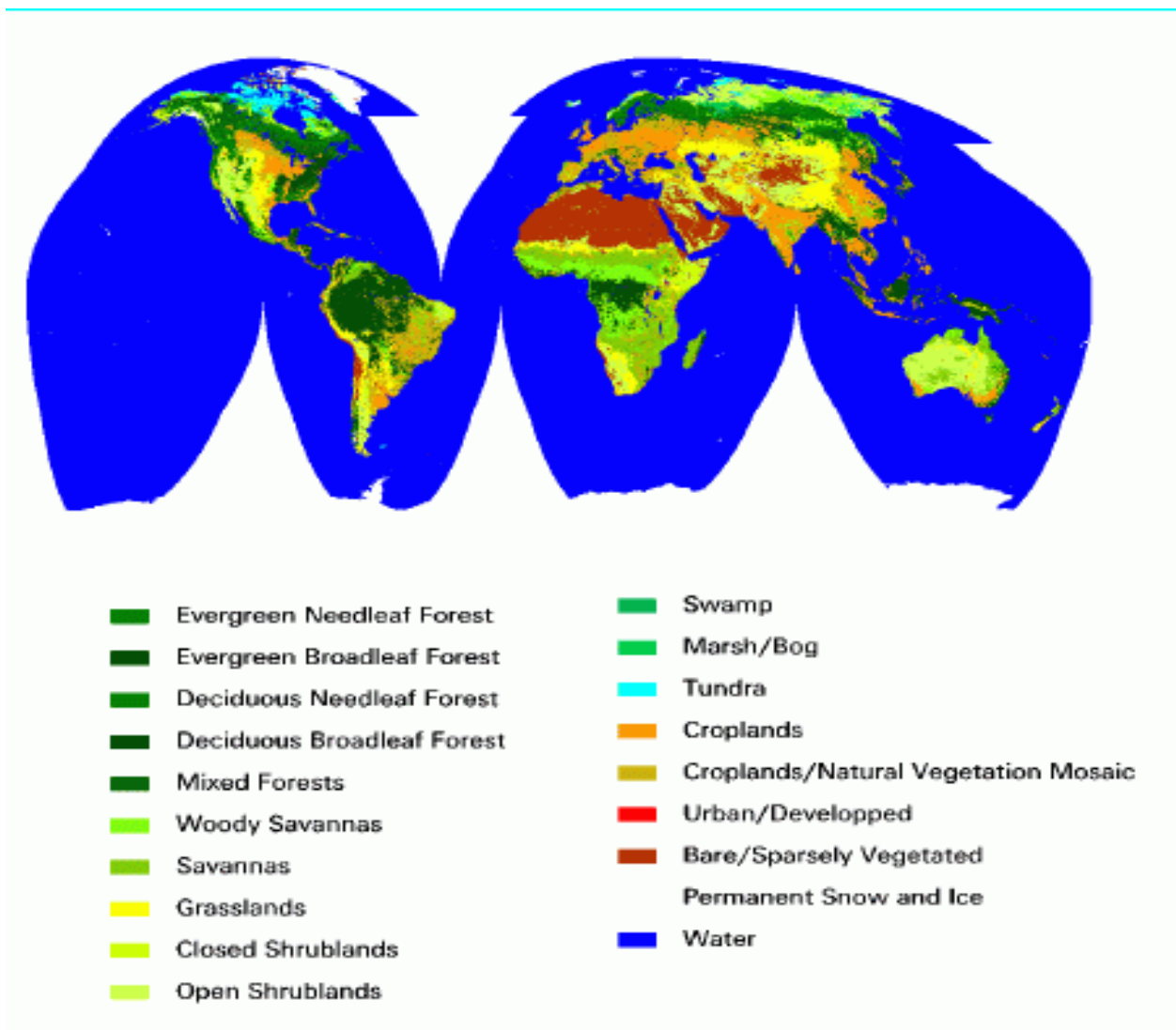
20

Figure 8. Global land cover distribution at 8km resolution in July 1992.
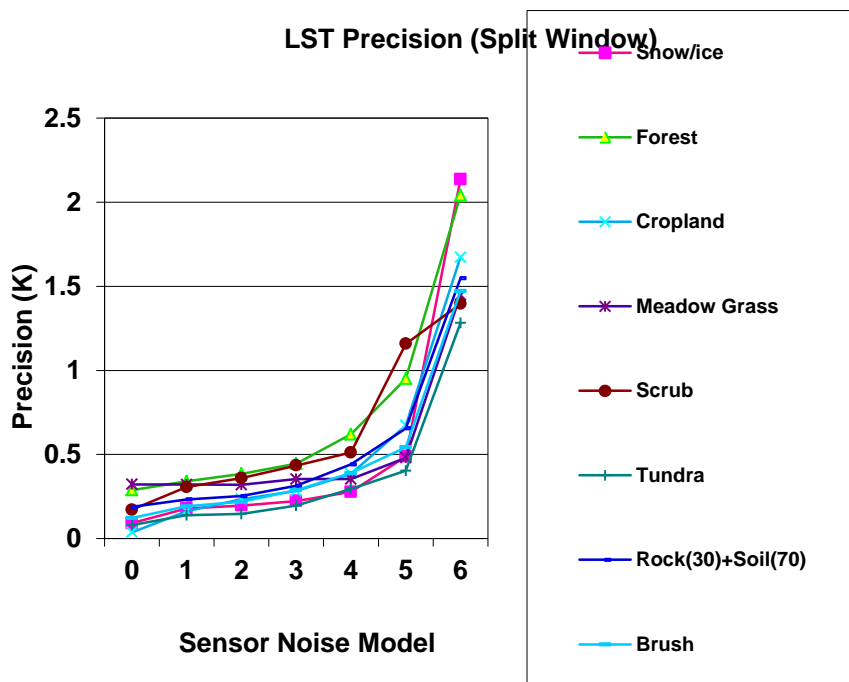
Figure 9a. Precision analysis for the VIIRS baseline split window (Land cover approach) retrieval method.
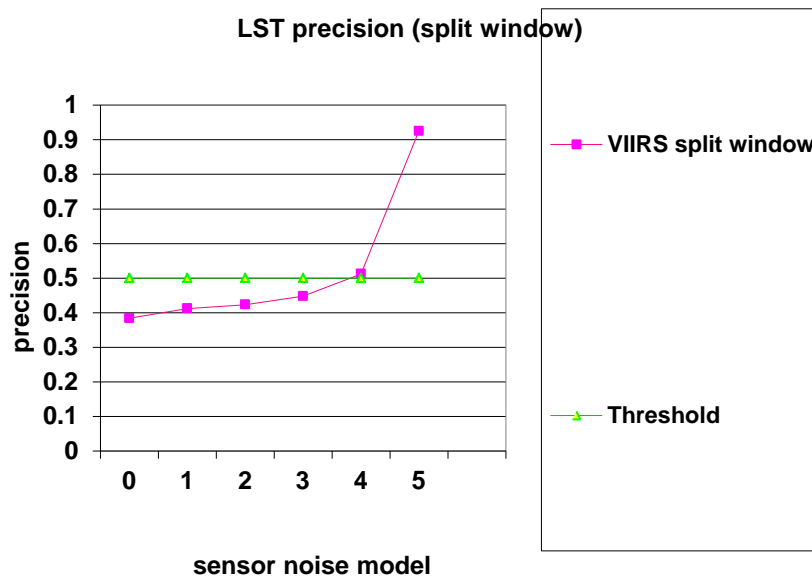
Figure 9b. Global LST retrieval precision for the VIIRS fallback split window (Land cover approach) retrieval method.
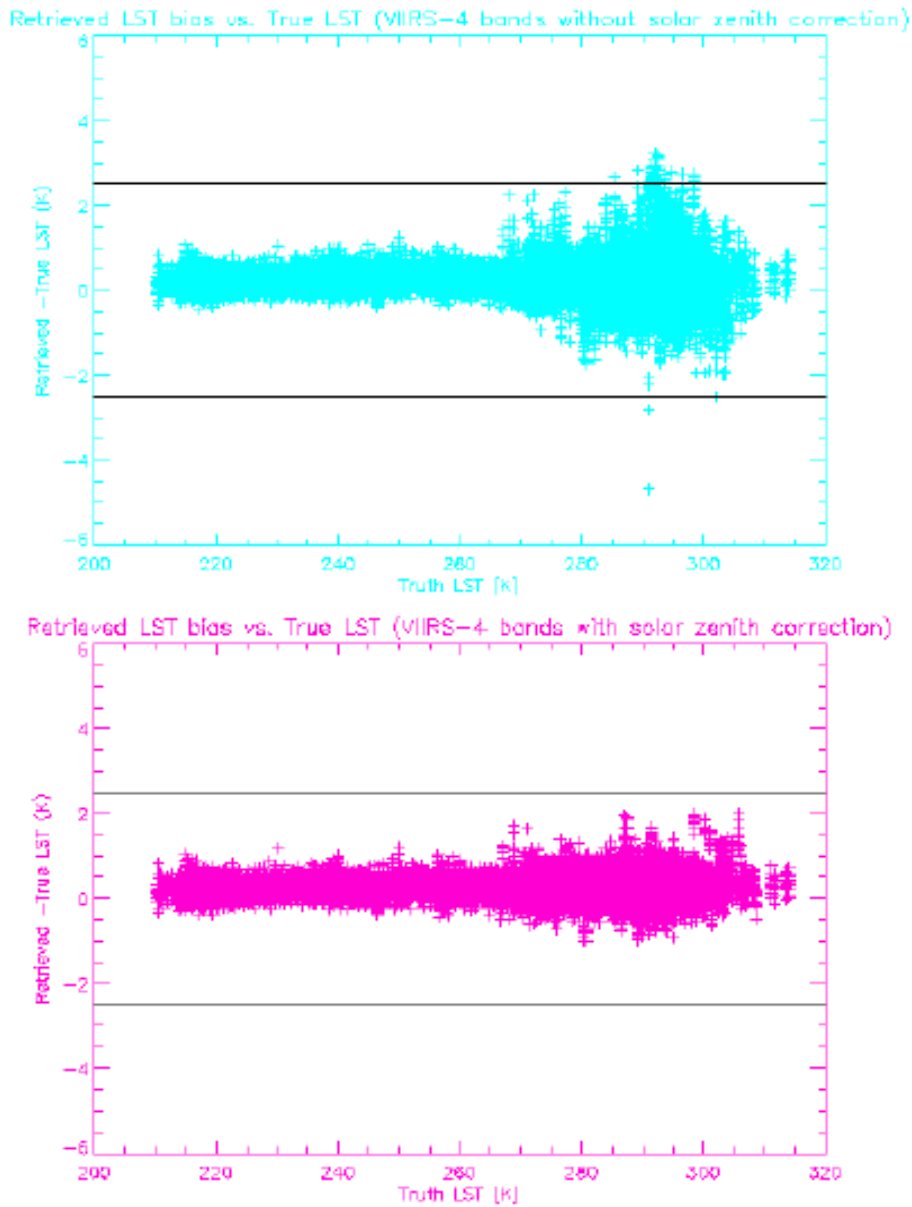
Figure 10. LST retrieval error vs. LST distribution for VIIRS dual split window algorithm (Land cover approach). The upper panel: Without solar zenith angle correction. The bottom panel: With solar zenith angle correction during the daytime.

Figure 11. Nighttime LST precision (upper panel), accuracy (middle) and uncertainty (bottom) distribution over satellite viewing angle and LST by using VIIRS dual split window algorithm (Land cover approach).
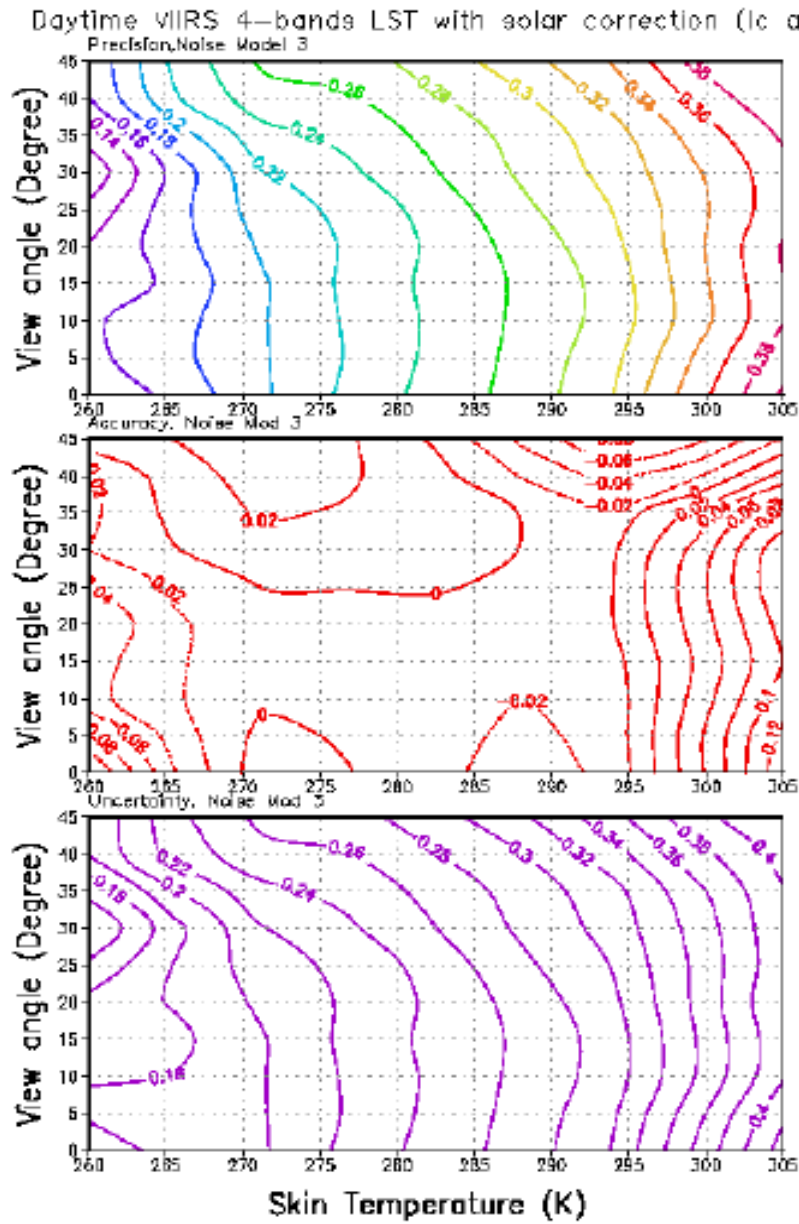
Figure 12. Daytime LST precision (upper panel), accuracy (middle) and uncertainty (bottom) distribution over satellite viewing angle and LST by using VIIRS dual split window algorithm (Land cover approach) with solar zenith correction.
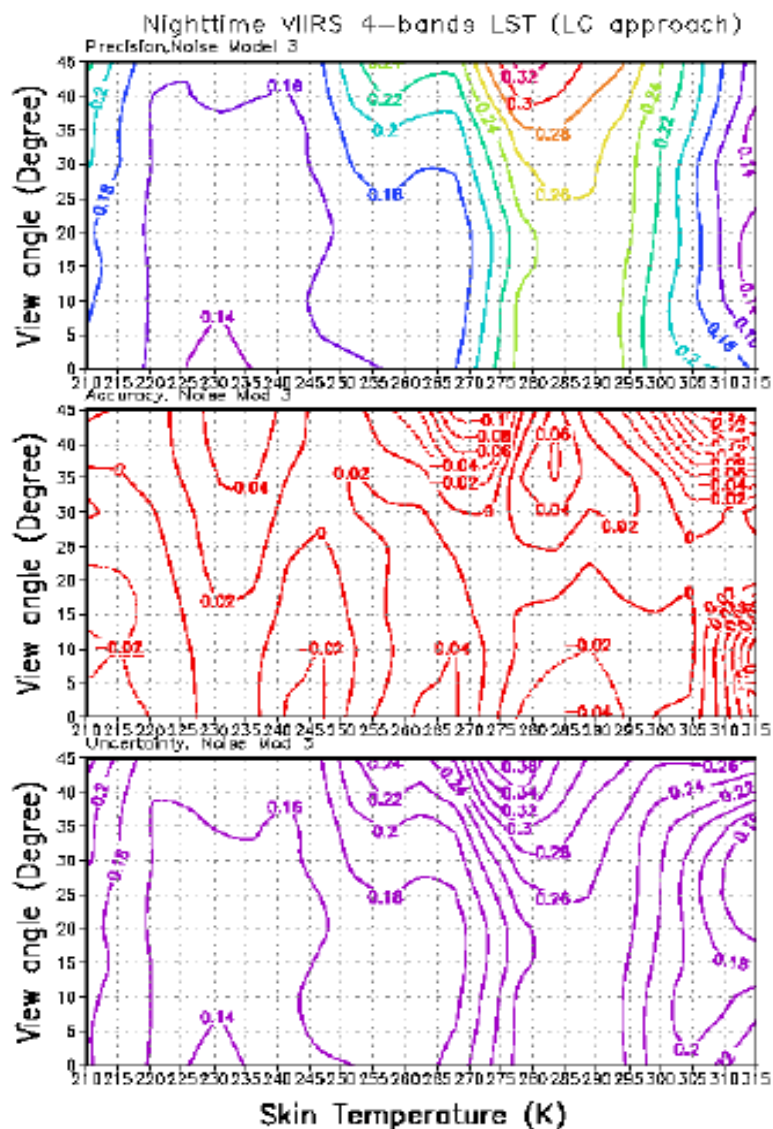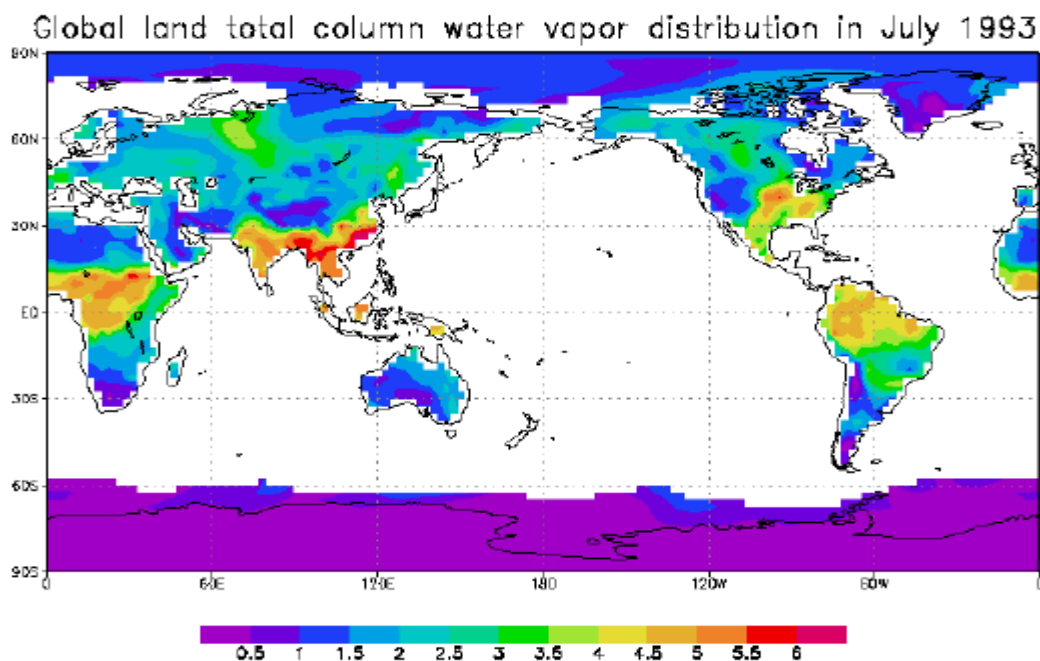
Figure 13. PW distribution over land in our global dataset.

Water vapor's effect

In window channels, the main atmospheric effect comes from the water vapor absorption. So the PW amount has important effect to LST retrieval error. Figure 13 show the PW distribution in this global dataset.

There is higher PW at higher temperature, as shown in Figure 14, and larger LST errors at warmer temperature above 280 K. We analyzed the relationship of LST retrieval error at temperature range 280-305 K with water vapor amount.

LST precision is worse at PW 0.5-1.0 g/cm^2. These retrievals correspond to rock, sand, desert or sea ice areas. Harris and Mason (1992) revealed that for a given change in surface temperature ΔT_0, the resulting changes in brightness temperatures in the two LWIR wavebands has the following relationship:

$$\frac{\Delta T_2}{\Delta T_1} = \frac{\varepsilon_2}{\varepsilon_1} \frac{\tau_2(\,0,\,p_0\,)}{\tau_1(\,0,\,p_0\,)}$$

$$\tau_\lambda(\,0, p_0\,) = exp(\,-k_{w\lambda} U_w(\,0, p_0\,)\,)exp(\,-k_{o\lambda} U_o(\,0, p_0\,)\,)$$

So surface emissivities changes, as well as atmospheric transmittance changes, cause brightness temperatures to change. If we divide the absorbing gases into water vapor and other gases:

$$\frac{\Delta T_2}{\Delta T_1} = \frac{\varepsilon_2}{\varepsilon_1} exp((k_{w1} - k_{w2})U_w(\,0, p_0\,))exp((k_{o1} - k_{o2})U_o(\,0, p_0\,)$$

where $k_{W\lambda}$ and KO_λ are the band–averaged absorption coefficients for water vapor and other gases, respectively; U_w $(0,p_0)$ and U_o $(0,p_0)$ are the total column contents of water vapor and other gases, respectively. Supposing that the magnitude $(k_{w1}-k_{w2})$ U_w $(0,p_0)$ is small, it is reasonable to take the first-order expansion, as U_w $(0,p_0)$ is the total column water or precipitable water W, so we have

$$\frac{\Delta T_2}{\Delta T_1} \approx \frac{\varepsilon_2}{\varepsilon_1} (1 + KW + const.)$$

So surface emissivity and atmospheric PW cause the brightness temperature to change and therefore cause LST retrieval error. At PW 0.5-1.0 g/cm^2, the emissivity changes for the 3.75 and 4.005 μm bands over rock, sand, and desert cause LST retrieval error.

The VIIRS dual split window algorithm (Land cover approach) shows LST precision can meet the threshold 0.5 K at all PW range and all viewing angles, shown as Figure 15. This is because this method overcomes the surface emissivity's effect.

Figure 14. Water vapor vs. surface skin temperature distribution.

Figure 15. The LST precision, accuracy and uncertainty distribution with the PW and viewing angle by using the VIIRS dual split window algorithm (Land cover approach).
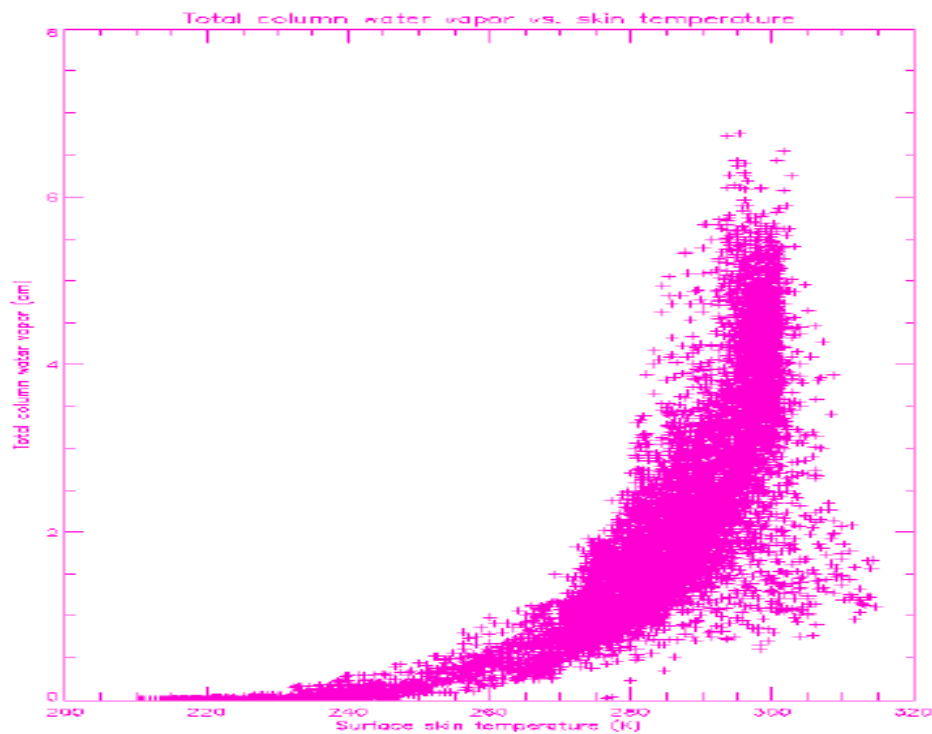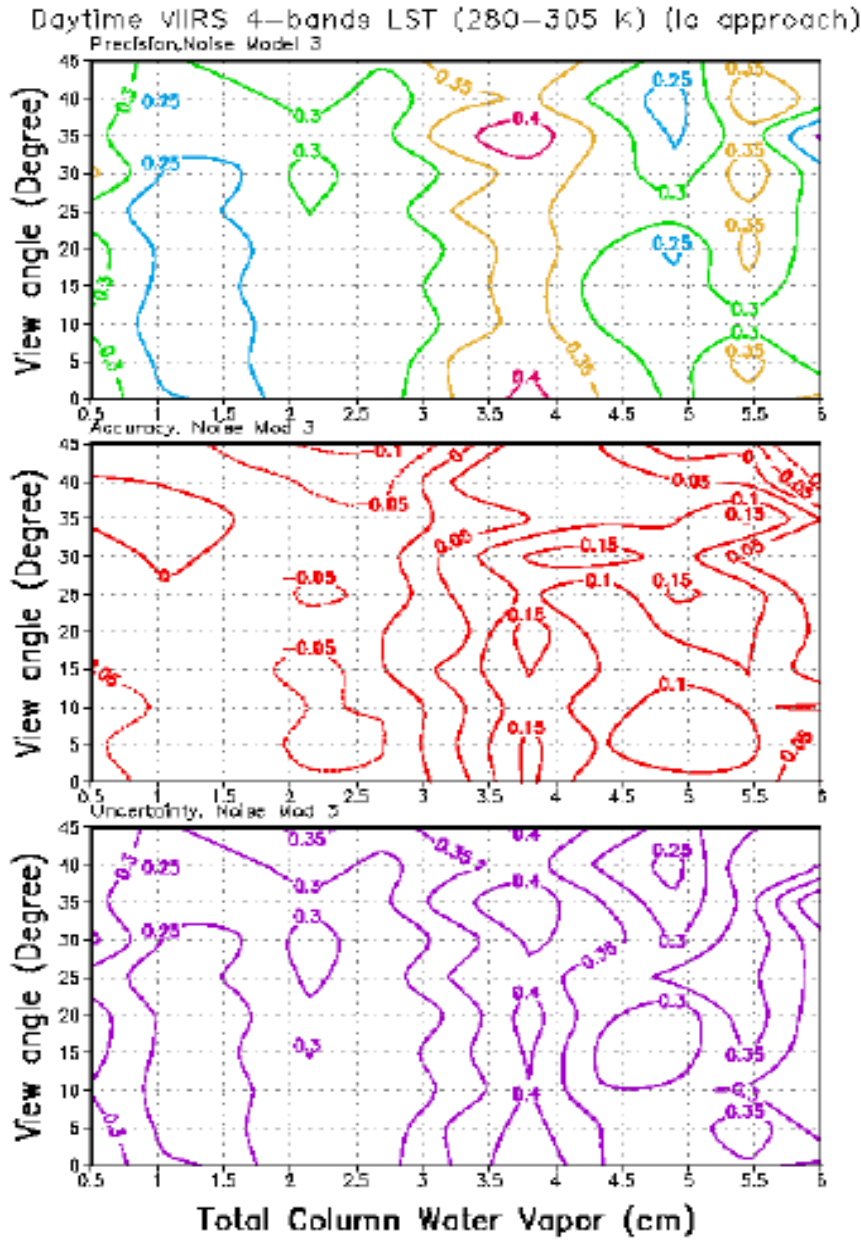
3.3.5 Validation problem

All of the tests above were performed based on simulation data, i.e., the truth LST was assumed to be known. For real-time data, the validation of global LST retrievals from satellite measurements is problematic since satellites measure skin temperature while ground truths provided by the global observational system are shelter temperatures. Although skin LSTs from a few field sites – such as the First International Satellite Land Surface Climatology Project (ISLSCP) Field Experiment (FIFE) – are now available (Prata, 1994; Wan and Snyder, 1996), they are not globally representative. Prata (1994) and many others have addressed the difficulty of obtaining ground truth LST. *In situ* LSTs can be measured with contact thermometers, as well as thermal infrared spectrometers. The contact thermometers measure LST at a point, while the satellites measure the mean LST over a pixel area. The LST may vary significantly within a pixel area, and therefore, a single pixel may require the use of a number of thermometers.

In reality, both spatial and time variability of land surface temperatures is greater than that of sea surface temperature. This makes the validation of LST retrieval from satellite data more difficult than with SST validation. Weng and Grody, (1998) tried to use shelter temperature in the early morning to validate LST retrieval from satellite SSM/I data. They found that the difference between surface skin temperature and shelter temperature is lowest at early morning. This validation, however, is limited to early morning. Another validation problem is the time. The number of *in situ* observations that match the satellite measurement in both time and space will be small: the *in situ* LST was not observed at the exact time when the satellite passed.

3.4 ALGORITHM SENSITIVITY STUDIES

3.4.1 Land Cover

The VIIRS split window algorithms depend on an accurate knowledge of land surface types. The VIIRS vegetation index EDR accuracy requirement is 70%. But, usually, accuracy above 80% can be achieved by using neural networks or decision tree algorithms. When we did an experiment with a 20% land cover classification error, the LST retrieval process is a little bit worse than the testbed results presented in this document, but the VIIRS dual split window LST algorithm can still meet the threshold of 0.5 K. This is because land cover classifications by using neural networks or decision trees misclassify to a similar surface type that still has similar emissivity characteristics. For instance, broadleaf forests may be misclassifying as pine forests, pine brush as broadleaf brush, or wet soil as scrub soil. Grass, however, is not likely to be misclassified as rock or sand. So this is why an algorithm based on surface types may not cause large errors, even with a 20% land cover classification error, see Figure 16.

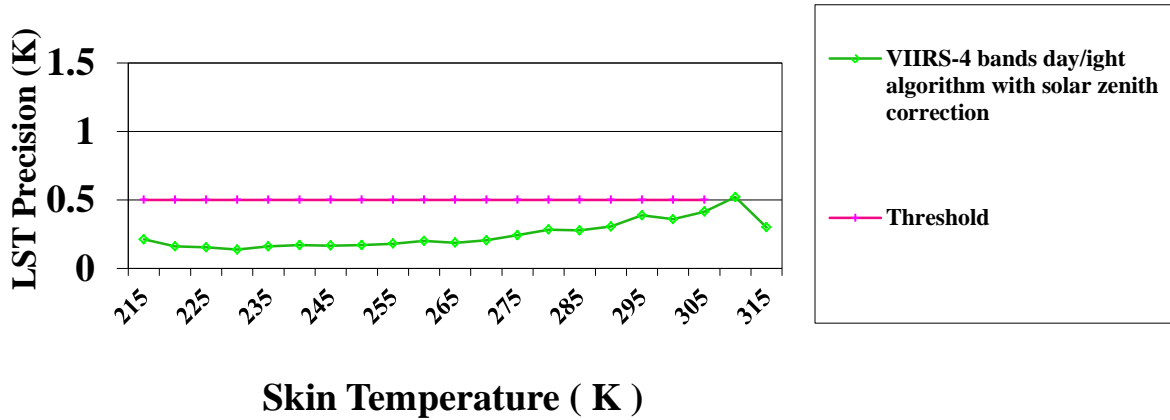**Precision v.s. Temperature and different algorithms for NCEP global data set with sensor noise model 3.**

Skin Temperature (K)

Figure 16. LST precision vs. temperature by using VIIRS dual split window day/night algorithm with 20% land cover classification error.

3.5 PRACTICAL CONSIDERATIONS

3.5.1 Numerical Computation Consideration

In order to retrieve LST within an operational timeframe, statistical algorithms that meet quality requirements have been developed that are much quicker than physical modeling methods. Pre-generated LUTs are used to speed processing yet retain flexibility.

3.5.2 Programming and Procedural Considerations

The simplicity of all the algorithms described in this document translates into very small amounts of code using basic mathematical routines. Computationally intensive processes are performed offline, with results delivered as re-generated LUTs. VIIRS Phase II efforts are largely software-focused, and the methodology for this development work is based on sound and proven principles, as discussed in the VIIRS Algorithm Software Development Plan *[Y6635]*. The present maturity of the VIIRS software is detailed in the VIIRS Algorithm Software Maturity Assessment document *[Y6661]*. The maturity and remaining Phase II tasks for the algorithms themselves is summarized in the VIIRS Algorithm/Data Processing Technical Report *[Y7040]*. The software designs relevant to the LST Unit are summarized in the VIIRS Context Level Software Architecture *[Y2469]*, Surface Temperature Module Level

32

Software Architecture *[Y2473]*, and Land Surface Temperature Unit Level Detailed Design *[Y2502]*. These designs are tested at the system level as described in the most recent versions of the VIIRS Software Integration and Test Plan *[Y3236]*, Algorithm Verification and Validation Plan *[Y3237]*, and System Verification and Validation Plan *[Y3270]*. A summary of the ultimate strategy for operational application of the system of VIIRS algorithms is provided in the VIIRS Operations Concept document *[Y2468]*. The VIIRS Interface Control Document (ICD *[Y2470]*) provides more detail on the specifics of ancillary data requirements for Vegetation Index and other VIIRS products.

3.5.3 Configuration of Retrievals

Adjustable parameters for the retrieval of the LST products allow post-launch updating of regression coefficients.   The flexibility built into the architecture also allows easy implementation of future P^3I developments.

3.5.4 Quality Assessment and Diagnostics

A number of parameters and indicators are reported in the LST product as retrieval diagnostic flags. Statistical information is reviewed for quality assessment. The LST EDR quality flags are derived from the NPP/NPOESS System Requirement. The lists of pixel level and granule level quality flags as well as their detailed description are given in the LST OAD (D38714) and are available in the NPP EDR Production Report, EDRPR (D37005). The detailed logic for setting the LST quality flags are described in the LST OAD (D38714). The logic for selection of the best quality LST pixels is also summarized in the LST OAD (D38714).

3.5.5 Exception Handling

Confident cloudy pixels identified by the cloud mask will be skipped. Pixels with poor quality SDR data will also be skipped and flagged.

3.6 ALGORITHM VALIDATION

3.6.1 Pre-Launch Validation

The regression coefficients for each IGBP land cover type, for day and night, for the optional dual split window algorithm and the baseline split window algorithm have been generated based on global synthetic data pre-launch. Verification and validation of the algorithms will be performed using global synthetic data and MODIS proxy data. The detailed description of both the global synthetic test data and the MODIS granulated test data, and the data generation process can be found in the NPP Operational Algorithm Proxy and Synthetic Test Data Description document [D45702].

3.6.2 Post-Launch Validation

The post-launch validation activities are designed primarily to test the LST retrieval algorithm. Several fundamentally different data sets are needed to provide an adequate sampling of the atmospheric conditions and LST to validate the VIIRS IR radiance and retrieved LST fields. Highly focused field experiments are necessary to understand the atmospheric processes that limit the accuracy of the retrieved LST. Sites will be selected globally to validate VIIRS LST retrieval. (MODIS LST ATBD, version 3.2). Relatively flat areas of highly unmixed surface type will yield the highest quality measurements for validation. Portable radiometers and a TIR spectrometer will be calibrated with the same blackbody radiation source. Long-term global data sets are necessary to provide a monitoring capability that would reveal calibration drift and the consequences of extreme atmospheric events. The sensitivity of the dual band split window algorithm to BBR and NFR sensor effects should be determined during the intensive calibration validation period when considering its use as a replacement to the two band split window algorithm as the baseline algorithm. Validation of the LST EDR performance is required over the lifetime of the NPOESS mission.

4.0   ASSUMPTIONS AND LIMITATIONS

A major limitation of the VIIRS LST retrieval is that it can only be done under clear sky conditions. Ground truth LST measurements are necessary for calibration and validation, but it is difficult to obtain true skin LST over the full range of land surface types. Typically, LST varies significantly on a sub-pixel scale, and over short timescales, so that satellite retrieved LST necessarily represents a pixel-averaged measurement at a snapshot in time.

5.0   REFERENCES

Becker, F. (1987): The impact of spectral emissivity on the measurement of land surface temperature from a satellite. *Int. J. Remote Sens*. 11: 369-394.

Becker, F., and Z. L. Li (1990). Toward a local split window method over land surface. *Int. J. Remote Sens*. 11, 369-393.

Becker, F., and Li, Z. -L. (1995) Surface temperature and emissivity at various scales: definition, measurement and related problems. *Remote Sens. Rev.* 12:225-253.

Berk, A., L. S. Bemstein, and D. C. Robertson (1987). MODTRAN: A moderate resolution model for LOWTRAN. Rep. GLTR-89-0122, Burlington, MA: Spectral Sciences, Inc.

Caselles, V., E. Valor, C. Coll, and E. Rubio (1997). Thermal band selection for the PRISM instrument 1. Analysis of emissivity-temperature separation algorithms. *J. Geophys. Res*., 102, 11145-11164.

Cornette, W. M., P. K. Acharya, D. C. Robertson, and G. P. Anderson (1994). Moderate spectral atmospheric radiance and transmittance code (MOSART). Rep. R-057-94(11-30), La Jolla, CA: Photon Research Associates, Inc.

Crag, R., M. Sugita, and W. Brutsaert, 1995: Satellite-derived surface temperature with boundary layer temperatures and geostrophic winds to estimate surface energy fluxes, J. Geophys. Rev., vol. 100, no. D12, 25447-25451.

Dozier, J., and Z. Wan (1994). Development of practical multiband algorithm for estimating land surface temperature from EOS/MODIS data. *Adv. Space Res*., 13, 81-90.

Harris, A. R., and I. M. Mason (1992). An extension to the split-window technique giving improved atmospheric correction and total water vapor. Vol. 13, no. 5, 881-892.

Jackson, R. D., R. J. Reginato, and S. B. Idso, 1977: Wheat Canopy temperature: a practical tool for evaluating water requirements, *Water Resour. Res*., vol. 13, 651-656.

Kimura, F. and A. P. Shimiru, 1994: Estimation of sensible and latent heat fluxes from soil surface temperature using a linear air land heat transfer model, *J. Appl. Meteorol*. , vol. 33, no. 4, 477-489.

Kealy, P. S., and S. J. Hook (1993). Separating temperature and emissivity in thermal infrared multispectral scanner data: Implications for recovering land surface temperature. *IEEE Trans. Geosci. Remote Sens*., 31, 1155-1164.

Kneizys, F. X., E. P. Shettle, L. W. Abreu, J. H. Chetwynd, G. P. Anderson, W. O. Gallery, J. E. A. Selby, and S. A. Clough (1988). Users guide to LOWTRAN7. Rep. AFGL-TR-88-0177, Bedford, MA: Air Force Geophys. Lab.

Li, Z. L., and F. Becker (1993). Feasibility of land surface temperature and emissivity determination from AVHRR data. *Remote Sens. Environ*, 43, 67-85.

Mannstein, H. (1987). Surface energy budget, surface temperature and thermal inertia in Remote Sensing Applications. In Meteorology and Climatology, ed. R. A. Vaughan and D. Reidel. I, NATO ASI Ser. C: Math. Phys. Sci. Vol 201, pp. 391-410, Dordrecht Netherlands: A Reidel Publishing Co.

Prata, A. J. (1993). Land surface temperature derived from the Advanced Very High Resolution Radiometer and the Along-Track Scanning Radiometer I. Theory. *J. Geophys. Res*., 98, 16689-16702.

Price, J. C. (1984), Land surface temperature measurements form the split window channels of the NOAA-7/AVHRR. J. Geophys. Res. 89: 7231-7237.

Running, S. W., 1991: Computer simulation of regional evapotranspiration by integrating landscape biophysical attributes with satellite data, in Land Surface Evaporation: Measurements and Parameterization, ed. T. J. Schmugge and J. C. Andre, New York: Springer-Verlag.

Running, S. W., C. Justice, V. Salomonson, D. Hall, J. Barker, Y. Kaufman, A. Strahler, A. Huete, J.-P. Muller, V. Vanderbilt, Z. Wan, and P. Teillet, 1994: Terrestrial remote sensing science and algorithms planned for EOS/MODIS, Int. J. Remote Sens., vol. 15, no. 17, 3587-3620.

Sellers, P. J., F. G. Hall, G. Asrar, D. E. Strebel, and R. E. Murphy (1998). The first ISLSEP Field, Experiment (FIFE). Bull. *Amer. Meteorol. Soc.,* Vol. 69, no. 1, 22-27, 1988.

Vidal, R. C. and B. L. Blad, 1991: Atmospheric and emissivity correction of land surface temperature measured from satellite using ground measurements or satellite data, Int. J. Remote Sens., vol. 12, no. 12, 2449-2460.

Wan, Z., and J. Dozier (1996). A generalized split-window algorithm for retrieving land-surface temperature from space. *IEEE Trans. Geosci. Remote Sens*., 34, 892-905.

Wan, Z., and W. Snyder (1996). MODIS Land-Surface temperature algorithm theoretical basis document. MODIS ATBD

Watson, K. (1992). Two temperature method for measuring emissivity. *Remote Sens. Environ*, 42, 117-121.

Weng, F., and N. Grody (1998), Physical Retrieval of land surface temperature using the special sensor microwave imager. *J. Geophys. Res*., 103: 8839-8848.

Yu, Y. D., A. Rothrock, and R. W. Lindsay, 1995: Accuracy of sea ice temperature derived from the advanced very high resolution radiometer, *J. Geophys. Res*., vol. 100, no. C3, 4525-4532.

Zhang, L., Lemeur, and J. P. Goutorbe, 1995: A one-layer resistance model for estimating regional evapotranpiration using remote sensing data, in Agricul. and Forest Meteorol., vol. 77, 241-261.